The dynamic viscoelastic characterisation and magnetic resonance imaging of poly(vinyl alcohol) cryogel

Crolla, J P; Britton, M M; Espino, D M; Thomas-Seale, L E J

DOI:
10.1016/j.msec.2021.112383

Document Version
Peer reviewed version

Citation for published version (Harvard):
Crolla, JP, Britton, MM, Espino, DM & Thomas-Seale, LEJ 2021, 'The dynamic viscoelastic characterisation and magnetic resonance imaging of poly(vinyl alcohol) cryogel: identifying new attributes and opportunities', *Materials Science and Engineering C*, vol. 129, 112383. https://doi.org/10.1016/j.msec.2021.112383

The Dynamic Viscoelastic Characterisation and Magnetic Resonance Imaging of Poly(Vinyl Alcohol) Cryogel: Identifying New Attributes and Opportunities

J.P. Crolla[1], M.M. Britton[2], D.M. Espino[1], L.E.J. Thomas-Seale[1]

[1]Dept. of Mechanical Engineering, University of Birmingham, Birmingham B15 2TT, UK

[2] School of Chemistry, University of Birmingham, Birmingham B15 2TT, UK

***Corresponding author**

JP Crolla
Dept. of Mechanical Engineering,
University of Birmingham,
Birmingham
B15 2TT
UK
Tel: +44(0) 121 414 3622
E-mail: j.p.crolla@bham.ac.uk

Abstract

Poly(vinyl alcohol) (PVA) cryogel is a biocompatible, synthetic hydrogel, compatible with magnetic resonance (MR) imaging . It is widely used as a biomaterial in tissue scaffolds and mimics to test various diagnostic techniques. The aim of this study is to characterise the effect of varying PVA concentration, molecular weight (MW) and manufacturing protocol on the viscoelastic mechanical properties and MR T_2 relaxation time. Further to this MR imaging (MRI) was investigated as a method to quantify material homogeneity. Cylindrical samples of PVA, of varying MW, concentration and number of freeze thaw cycles (FTCs), were manufactured. Dynamic mechanical analysis was performed to evaluate the storage and loss moduli between frequencies of 0.5 and 10 Hz. MR T_2 relaxation maps were imaged using a 7 T MRI instrument. Storage and loss moduli were shown to increase with MW, concentration, or the number of FTCs; with storage modulus ranging from 55 kPa to 912 kPa and loss modulus ranging from 6 kPa to 103 kPa. MR T_2 relaxation time was shown to increase linearly with PVA concentration. The qualitative and quantitative heterogeneity of the PVA sample were identified through MR T_2 relaxation time maps. Excitingly, PVA demonstrated a composition-dependent casual correlation between the viscoelastic mechanical properties and MR T_2 relaxation time. In conclusion, this research thoroughly characterised the viscoelastic mechanical properties of PVA to support its extensive use as a biomaterial, and demonstrated the use of MRI to non-invasively identify sample heterogeneity and to predict the composition-dependent viscoelastic properties of PVA.

KEYWORDS: Biomaterials; MRI; Loss Modulus; PVA; Storage modulus.

1. Introduction

Poly(Vinyl Alcohol) (PVA) is a widely used biomaterial [1, 2], particularly prevalent as a component of tissue scaffolds and a tissue mimicking material. The development of biomaterials, including PVA, for novel clinical applications offers significant social and economic impact. For example, connective tissue (e.g. arterial, articular cartilage and bone) damage impacts on the quality of life, and life expectancy of a large percentage of the world population [3, 4]. Cardiovascular Disease (CVD) was responsible for 164,000 deaths in the UK in 2019, and accounts for 27% of total deaths recorded [5]. Osteoarthritis (OA), a degenerative disease of synovial joints, is another prevalent example of connective tissue damage. In the USA, 1.5M hip and knee joint replacements were predicted for 2020, compared to 700,000 performed in the US in 2012 [6]. It is apparent that the clinical impact of connective tissue damage and disease is heavy and ever increasing. The surgical intervention, often required to repair or replace damaged tissue, poses an enormous and increasing cost to the worldwide economy. In 2017, cardiovascular disease cost the UK economy £28 billion [3]. The total cost of CVD in the USA was $555 billion in 2016; in line with increasing population and obesity rates, this figure is projected to be $1.1 trillion per year by 2035 [4]. PVA is also used as a tissue mimicking material. Tissue mimicking phantoms are an efficient and cost effective method of experimentally simulating the design, development and testing novel diagnosis or intervention techniques whilst avoiding the use of animal tissue. PVA is particularly well known as a vessel mimicking material and forms an essential tool in the research of cardiovascular biomechanics, diagnostic CVD techniques and medical device testing [7-9].

PVA cryogel consists of a mixture of PVA and water, it is physically cross-linked through one or more freeze-thaw cycles (FTCs). PVA cryogel is a biocompatible, synthetic, polymer with variable mechanical properties that depend on concentration, molecular weight, and the

67 temperature, duration, and number of FTCs during manufacture. This allows the material to
68 replicate a broad-spectrum of soft tissues [10, 11], and has led to its frequent application as a
69 component of heart valve stents [10], prostheses [9], intervertebral disc prostheses [12], as a
70 material for articular cartilage replacement [13-17], and to model the mechanical properties
71 of super-soft biological materials such as brain and lung tissue [18]. Furthermore, it is widely
72 applied as a vessel mimicking material for cardiovascular phantoms [7, 19-21].
73 It is clear that PVA cryogels are used for numerous applications and possess the distinctive
74 advantages that the mechanical properties can be designed through manufacturing. Yet, the
75 extensive use of PVA, and ultimately the clinical translation, must be supported by relevant
76 and thorough mechanical and chemical characterisation. To date, there are some key
77 omissions in research literature which aim to characterise this biomaterial.
78 The majority of soft tissues in the body are viscoelastic [22-24], including connective tissue
79 [25], therefore mechanical viscoelastic characterisation is crucial to under pin any research
80 involving PVA tissue scaffolds or mimics. It has been reported in the literature that PVA
81 exhibits viscoelastic properties [26-28], yet it has not yet been characterised using dynamic
82 mechanical analysis (DMA). DMA measures dynamic viscoelasticity; characterising a
83 material in terms of its ability to store energy (storage modulus) and its ability to dissipate
84 energy (loss modulus). An induced stress results in instantaneous strain (the elastic response)
85 and a time-dependent strain (the viscous response). This characterisation technique is
86 analogous to in-vivo dynamic loading, and as such, is a crucial methodology to describe the
87 mechanical response of the material.
88 PVA can be imaged by magnetic resonance (MR) imaging (MRI) using the nuclear magnetic
89 resonance (NMR) signal of the water within the material. This is regarded as an important
90 characteristic, particularly in its application as a vessel mimicking material [21, 29]. Chu et
91 al. [29] demonstrated, for a fixed concentration, the change in MR T_1 and T_2 relaxation times

with FTCs. Orr et al. [30] showed the effect of PVA concentration and temperature on the MR T_1 and T_2 relaxation times, using a 3T MRI instrument. In these studies, the relationship between manufacturing parameters and MR relaxation is incomplete. This study will investigate MW, concentration and FTCs simultaneously, and thus, it will comprehensively support the dynamic mechanical analysis. Neither of these previous studies [29, 30] were able to confirm sample homogeneity, due to the lower spatial resolution, typical of clinical MRI instruments. This research will apply a high-resolution micro-imaging instrument (7 T) and thus determine the impact of the manufacturing protocol on the sample homogeneity.

In summary, this research will mechanically and chemically characterise PVA cryogel against compositional and manufacturing parameters, which to date have not been addressed in research literature. The study aims to characterise the effect of composition against MW and number of FTCs on the viscoelastic mechanical properties and the MR T_2 relaxation time of PVA. Furthermore, this study will assess the change in the homogeneity of PVA samples during manufacture. The resulting viscoelasticity and MR T_2 relaxation times are crucial to fully understanding the application of the biomaterial to tissue scaffolds and mimics, and underpin future clinical translation.

2. Methodology

2.1 Sample Preparation

Cylindrical specimens with dimensions of 20 mm diameter and 10 mm height were used for all DMA and MRI analyses. The specimen size was chosen to give the maximum surface area to assess the heterogeneity of PVA compositions through MR Imaging (relative to the core of the instrument). PVA was acquired from Sigma Aldrich (St Louis, Missouri, USA) and had a hydrolysis of 99+%. To incorporate the range of molecular weights (MW) of PVA this study utilised two different MWs; 89-98 kDa and 146-186 kDa. Each MW was manufactured at

concentrations of 10, 15, 17.5, and 20 %. A total of 72 samples (six samples for each composition of PVA) were used for mechanical testing; with another 36 (three samples per composition of PVA) samples used for imaging.

Table 1: Reference table for molecular weight, freeze thaw cycles, and concentrations of PVA compositions used in this study.

Composition reference	Molecular Weight (kDa)	No. Freeze thaw cycles	Concentrations (% w/w)
PVA-A	89-98	3	10
			15
			17.5
			20
PVA-B	146-186	1	10
			15
			17.5
			20
PVA-C	146-186	3	10
			15
			17.5
			20

PVA powder was stirred into distilled water, covered (to reduce evaporation) and stirred using an automatic overhead stirrer, at 90 ºC for one hour, where upon it was fully dissolved. The mixture was stirred for another 1 hour, to retain homogeneity, whilst the solution was allowed to cool down to room temperature. The solution was poured into cylindrical moulds and then underwent 3 FTCs. The FTC process consisted of three phases across 24 hours; 12 hours in the freezer at -20ºC, 4 hours in the freezer without active cooling (to increase temperature gradually), and finally 8 hours at a room temperature of 22 ± 1 °C. After the required FTCs, the samples were stored in distilled water for three days to reach hydrostatic equilibrium. Each MW and all concentrations were assessed after 3 FTCs. Molecular weight 146-186 kDa was assessed at 1 FTC. Molecular weight 89-98kDa was not assessed at 1 FTC due to low stiffness.

2.2 Experimental Protocol

2.2.1 Magnetic Resonance Imaging

MR images of 3 PVA samples at four different concentrations of PVA-A, PVA-B, and PVA-C, were collected using a Bruker Biospin DMX-300 spectrometer (Bruker UK Limited, Coventry, UK) operating at a proton resonance frequency of 300.13 MHz. A Micro 2.5 imaging probe, with a 25 mm ^{1}H quadrature Radio Frequency (RF) coil, was used for all experiments. MR T_2 relaxation maps were determined from a series of 8 echo images using the spin-echo imaging sequence RARE (Rapid Acquisition with Relaxation Enhancement) [30]. Images were collected using a 128 × 128 pixel array, 25 × 25 mm^2 field of view and a slice thickness of 1 mm. MR T_2 relaxation maps were calculated using a repetition time (T_R) of 15,000 ms, with a RARE factor of 8.

To quantify the difference between the number of FTCs, and storage in water on the MR T_2 relaxation time of PVA, nine samples of 10% 146-186 kDa PVA were imaged immediately post-thawing, after 1 and 3 FTCs without storage in water (*Figure 1*). They were then allowed to reach equilibrium in distilled water for three days, and subsequently imaged again. These samples were not mechanically tested in order to remove any additional variables which may alter their MR T_2 relaxation time.

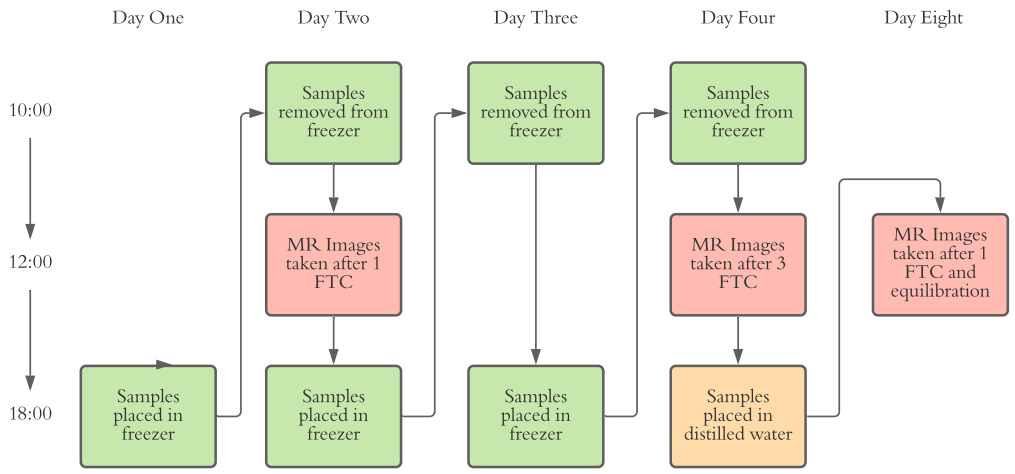

Figure 1: Flow-chart showing protocol used to assess the effect of 3 repeat freeze thaw cycle and equilibration on T_2 relaxation time

2.2.2 Dynamic Mechanical Analysis

A Bose Electroforce 3200 (Bose Corporation, ElectroForce systems Group, Minnesota, USA; now TA Instruments, Delaware, USA) mechanical testing machine, running Wintest software (TA Instruments, Delaware, USA) was used to perform all DMA. A sinusoidal displacement (d) was applied to the samples, and corresponding load (F) and phase lag (δ) were measured. A Fast Fourier Transform (FFT) of both the load (F^*) and displacement (d^*) was then performed, with the ratio between their respective data-set lengths giving a dynamic stiffness (K^*); equation 1. The storage (k') and loss (k'') stiffness were then calculated using equations 2 and 3. The sample diameter (D), and height (h) were measured for all samples in order to calculate their shape factor (S); which for a cylinder is given by equation 4. The storage (E') and loss (E'') moduli were then calculated using equations 5 and 6, respectively. This method is consistent with characterising the dynamic viscoelasticity of natural and synthetic biomaterials [22, 24].

$$K^* = \frac{F^*}{d^*} \qquad (\boldsymbol{Eq.1})$$

$$k' = k^* \cos(\delta) \qquad (\boldsymbol{Eq.2})$$

$$k'' = k^* \sin(\delta) \qquad (\boldsymbol{Eq.3})$$

$$S = \frac{\pi D^2}{4h} \qquad (\boldsymbol{Eq.4})$$

$$E' = \frac{k'}{S} \qquad (\boldsymbol{Eq.5})$$

$$E" = \frac{k"}{S} \qquad (\boldsymbol{Eq.6})$$

Samples were compressed by 20% of their measured height using a frequency sweep of 0.5 – 10 Hz. This frequency range was chosen to replicate the strain rates expected in different connective tissues; such as coronary arteries (0.5-10 Hz) [24], heart valve leaflets (0.5-10 Hz) [31], chordae tendineae (0.5 – 10 Hz)[32], and articular cartilage under physiological loading (1 – 10 Hz) [33]. A preconditioning cycling of 5 Hz for 60 seconds was run prior to each test

to negate the effects of stress relaxation. Complex moduli can be calculated from storage and loss moduli using equation 7 (note it is not included in the results or supplementary sections to avoid repetition of data).

$$E^* = \sqrt{E'^2 + E''^2} \qquad (\boldsymbol{Eq.7})$$

2.2.3 Data Analysis

All statistical analyses were performed using SigmaPlot (SYSTAT, San Jose, CA, USA). Data has been represented as mean ± standard deviation (SD) unless otherwise stated. Regression analysis has been used to empirically fit trendlines for comparisons between viscoelastic properties (storage, E' and loss, E'' moduli) and concentration (equations 8 and 9); MR T_2 relaxation rate, MR R_2 and concentration (equation 10); and viscoelastic properties and MR T_2 relaxation rate (equations 11-14). All the constants of the equations for regression and coefficients of determination (R^2) for trend lines are given in supplementary data.

$$E' \text{ , } E'' = a + be^{dC} \qquad (\boldsymbol{Eq.8})$$

Where a_s, b_s, and d_s are constants for E'; and a_l, b_l, and d_l are constants for E''; and C is the concentration of PVA.

$$E' = f + gC \qquad (\boldsymbol{Eq.9})$$

$$R_2 = x + yC \qquad (\boldsymbol{Eq.10})$$

$$E'_A = a_s + b_s e^{d_s R_2} \qquad (\boldsymbol{Eq.11})$$

$$E'_B = a_s + b_s R_2. \qquad (\boldsymbol{Eq.12})$$

$$E''_A = a_l + \ b_l e^{\ d_l R_2} \qquad (\boldsymbol{Eq.13})$$

$$E''_B = a_l + \ b_l R_2. \qquad (\boldsymbol{Eq.14})$$

A one way ANOVA was used to ascertain whether a statistically significant difference between the loss moduli of 15, 17.5 and 20% PVA-C was present. Results with $p < 0.05$ were considered significant.

3. Results

3.1 Dynamic viscoelasticity and composition of PVA

3.1.1 PVA Concentration and viscoelastic properties

Storage Modulus

An increase in PVA concentration from 10-20% resulted in an increase in Storage modulus at all frequencies (Figure 2); this was the case for the three compositions of PVA (A, B, C). For example, for PVA-A tested at 0.5 Hz, the storage modulus increased from 158 ± 9.5 kPa at 10% concentration to 484 ± 24 kPa at 20% concentration. Frequency affected all compositions in a similar manner, with an increase in storage modulus as the frequency was increased. For PVA-A, between 0.5 and 10 Hz, average increases of 8.2, 8.1, 15, and 13% were calculated for 10, 15, 17.5, and 20% concentrations.

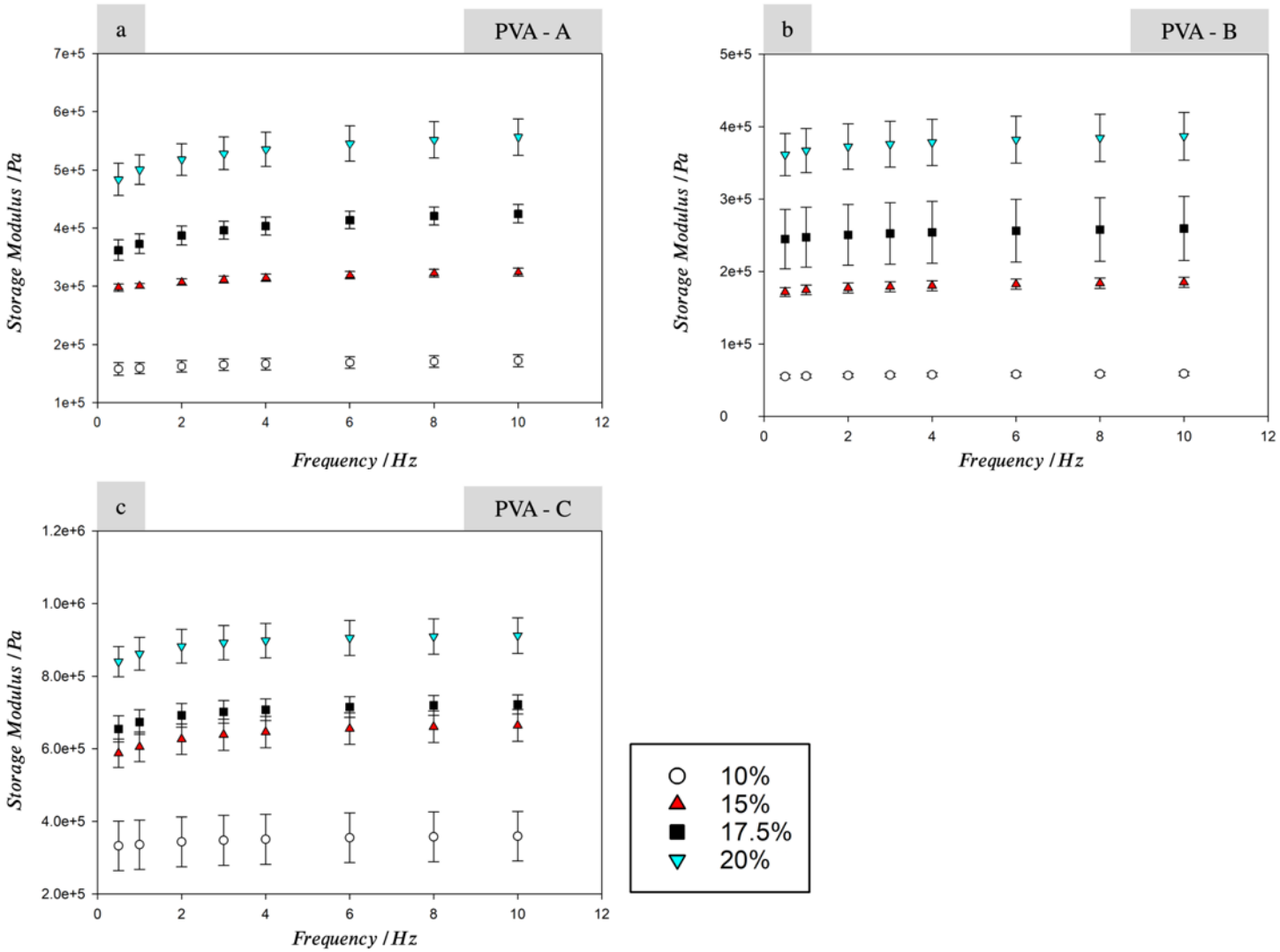

Figure 2: Storage modulus for PVA-A (a), PVA-B (b), and PVA-C (c), at concentrations of 10, 15, 17.5 and 20% w/w. Error bars show 95% confidence intervals (n = 6).

211 An exponential relationship was evident between storage modulus and concentration for

212 PVA-A ($R^2 = 0.99$) and PVA-B ($R^2 = 0.96$) (Figures 3a and 3b). This differed to the linear

213 relationships shown by PVA-C ($R^2 = 0.94$) (Figure 3c). These relationships were apparent for

214 all frequencies.

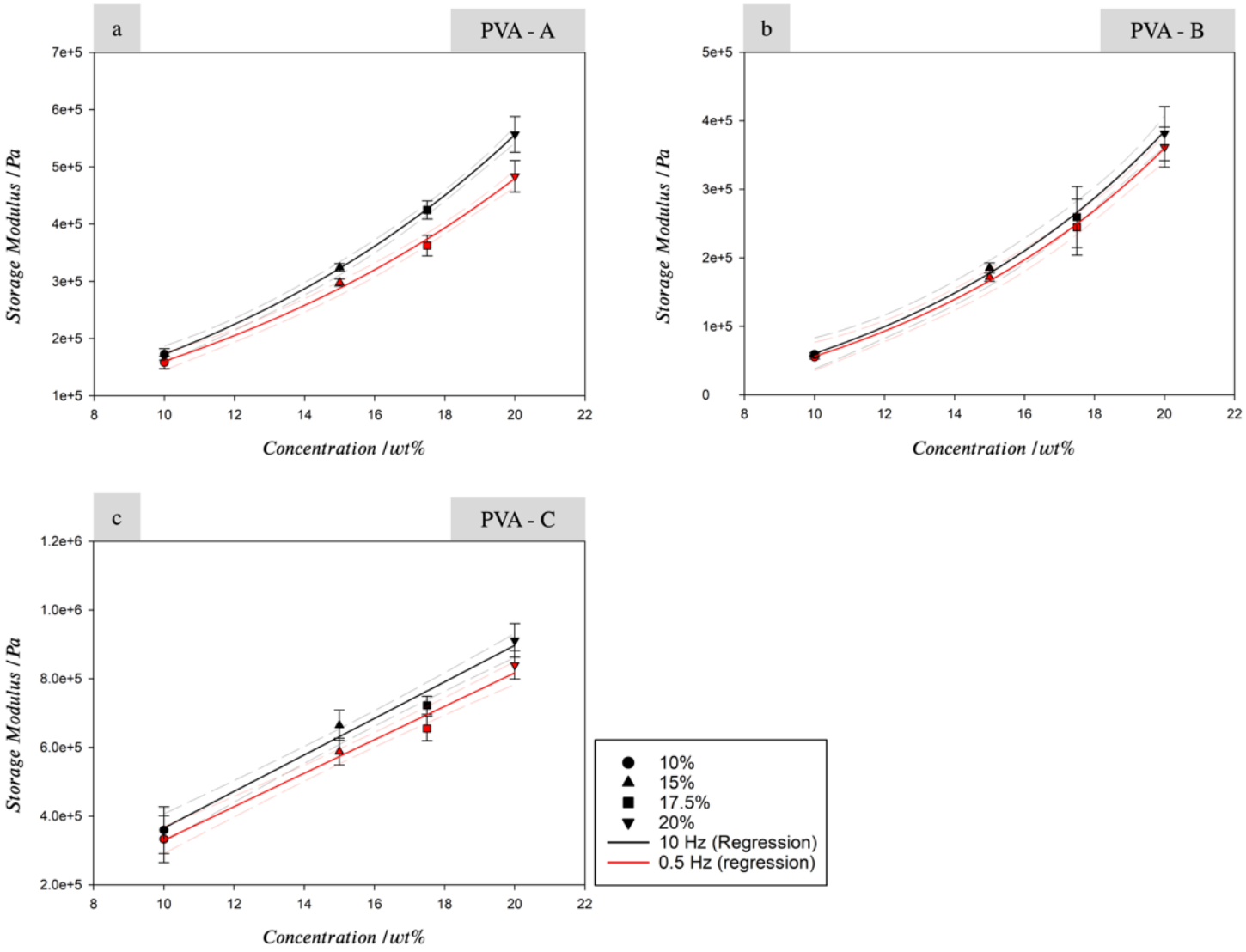

Figure 3: Storage Modulus plotted against concentration for 0.5 Hz (red), and 10 Hz (black) for PVA-A (a), PVA-B (b), and PVA-C (c). Error bars show 95% confidence (n= 6). Regression lines for 0.5 Hz (red), and 10 Hz (black) are also given; dashed lines show 95% confidence intervals for regression.

215

216

217

218

Loss Modulus

For all samples, loss modulus was found to be lower than storage modulus. For PVA-A and B, a similar relationship was seen between loss modulus and PVA concentration, with an increase in concentration resulting in an increase in loss modulus at all frequencies tested (Figure 4). For example, for PVA-A tested at 0.5 Hz, an increase from 25.4 ± 2.3 kPa at 10% concentration to 86.5 ± 2.3 kPa at 20% concentration was measured. A large increase in loss modulus was seen at all frequencies between 10 and 15% concentration for PVA-C (increasing from 38.1 ± 5.4 kPa to 87.8 ± 11 kPa at 0.5 Hz, and 39.9 ± 3.0 kPa to 73.1 ± 13 kPa at 10 Hz). However, no statistically significant difference was seen between 15, 17.5 and 20% at any frequency ($p = 0.53 \pm 0.25$) (Figure 4).

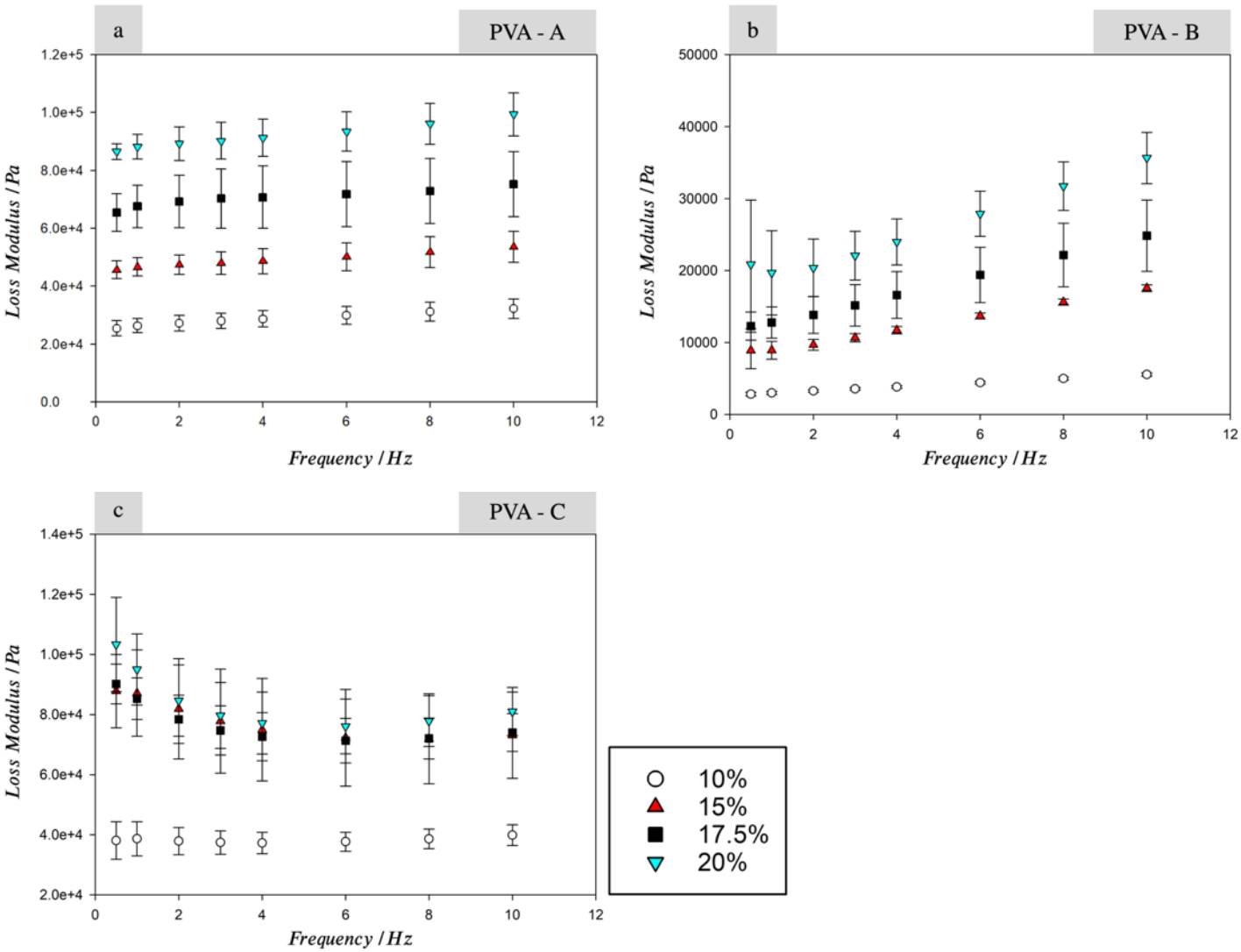

Figure 4: Loss modulus for PVA-A (a), PVA-B (b), and PVA-C (c), at concentrations of 10, 15, 17.5 and 20% w/w. Error bars show 95% confidence intervals (n = 6).

229

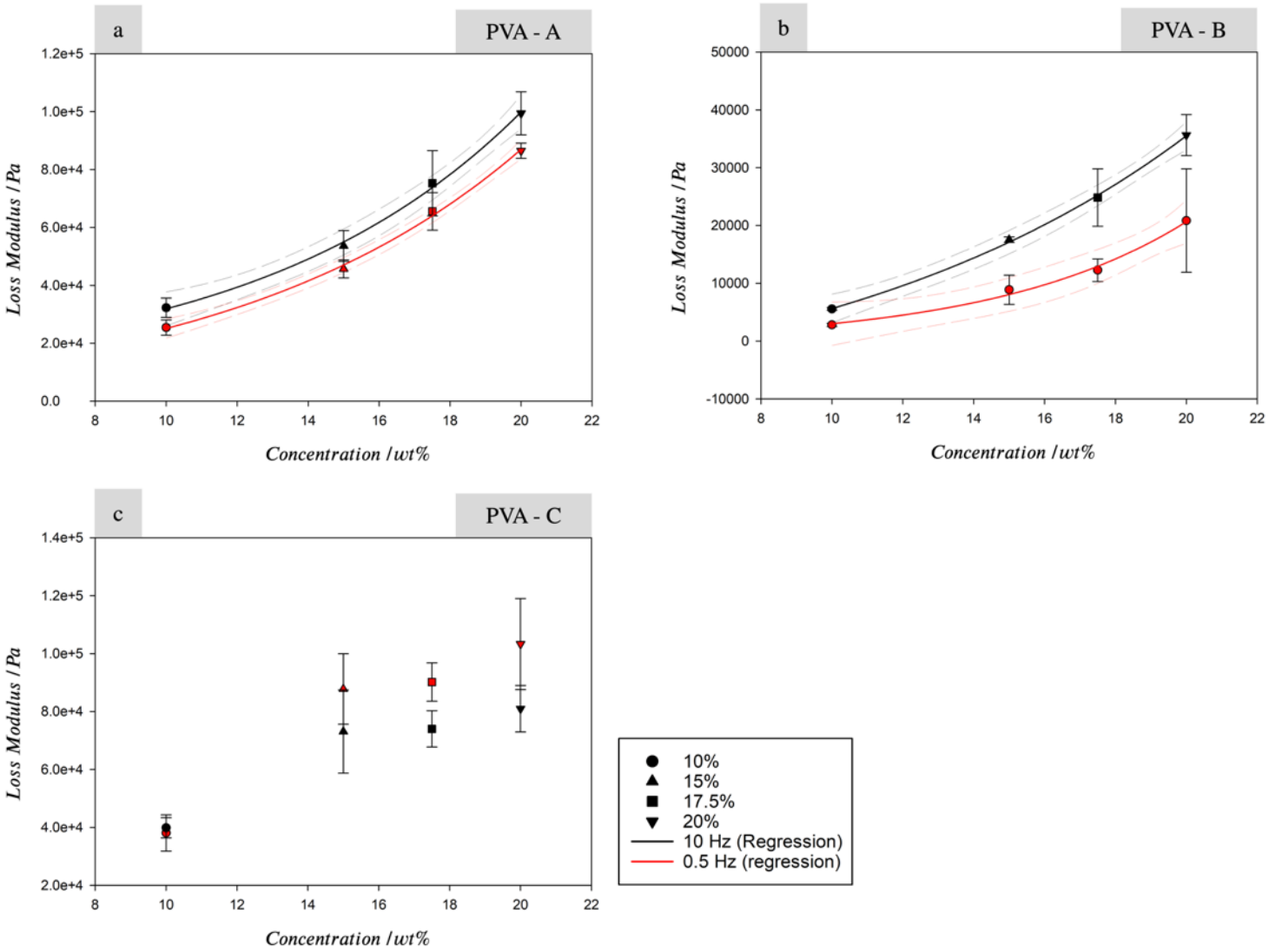

Figure 3: Loss Modulus plotted against concentration for 0.5 Hz (red), and 10 Hz (black) for PVA-A (a), PVA-B (b), and PVA-C (c). Error bars show 95% confidence (n= 6). Regression lines for 0.5 Hz (red), and 10 Hz (black) are also given; dashed lines show 95% confidence intervals for regression.

230 Frequency was shown to impact loss modulus; for PVA-A between 0.5 and 10 Hz, average
231 changes of 22%, 4.8 %, 10%, and 7.8% were seen at 10 ,15, 17.5, and 20% w/w, respectively.
232 A more consistent increase of 49, 49, 50, and 41% at each concentration was seen for PVA-
233 B. For PVA-C, a change of 0.1% was seen at 10%, and a decrease of 20, 21, and 27% was
234 seen for 15, 17.5, and 20% w/w, respectively. An exponential relationship was derived
235 empirically between the loss modulus and concentration for PVA-A ($R^2 = 0.95$) and PVA-B

236 ($R^2 = 0.91$) (Figures 5a and b). However, a similar relationship was not observed for PVA-C
237 (Figure 5c), thus no trend line has been empirically fitted.

238 ***3.1.2 Molecular weight of PVA and viscoelastic properties.***

239 The Storage modulus increased for all concentrations of PVA with increasing molecular
240 weight, from 89-98 kDa to 146-186 kDa (Figures 2a and 2c). This increase was observed for
241 all frequencies, with an average of a 2.1 × increase at 10% w/w concentration; 2.0 × at 15%
242 w/w concentration; 1.8 × at 17.5% concentration; and 1.7 × at 20% concentration. As stated
243 in section 3.1.1, the frequency dependency of storage modulus showed little change, and both
244 compositions could be empirically characterised using an exponential trend line to compare
245 storage modulus and PVA concentration (Figures 3a and 3c).
246 An increase in loss modulus was also observed for 10, 15, and 17.5% at all frequencies. An
247 average increase of 1.3 × at 10% w/w concentration; 1.6 × at 15% w/w concentration; 1.1 ×
248 at 17.5% concentration. A decrease of 0.91 × was noted for 20% w/w concentration. As per
249 section 3.1.1, the frequency dependency of the loss modulus was shown to be different for the
250 two MWs of PVA, with the loss modulus increasing with respect to frequency for PVA-A,
251 and decreasing for PVA-C. It was also previously noted that no significant trend could be
252 used to describe the effect of concentration on loss modulus for the higher MW PVA, as
253 compared to lower MW PVA concentrations where the trend could be empirically
254 characterised using an exponential trend line.

255 ***3.1.3 Freeze thaw cycles on viscoelastic properties.***

256 The storage modulus increased for all concentrations of PVA with an increase from 1 to 3
257 FTCs (Figures 2b and 2c). This increase was observed for all frequencies, with an average 6.1
258 × increase at 10% w/w concentration; 3.5 × at 15% w/w concentration; 2.8 × at 17.5%
259 concentration; and 2.4 × at 20% concentration.

An increase in loss modulus was also observed for all samples at all frequencies when the number of FTCs was increased. However, smaller increases were seen at higher frequencies for each concentration. This decrease varied from 14 × at 0.5 Hz to 7.2 × at 10 Hz at 10% w/w concentration; 9.9 × to 4.2 × at 15% w/w concentration; 7.3 × to 3 × at 17.5% w/w concentration; and 4.9 × to 2.3 × at 20% w/w concentration. The inter sample variation increased for 10% PVA when the number of FTCs was increased to 3. With SD being 2.8 ± 0.08% of the mean after 1 FTC, and 17 ± 0.4% of the mean after three cycles.

3.2 MRI and composition of PVA

3.2.1 Molecular Weight, Concentration and MR T_2 Relaxation Time.

MR T_2 Relaxation time was shown to decrease as concentration of PVA was increased from 10 to 20% (Table 2). The plot of MR T_2 relaxation rate against concentration for all compositions shows a linear relationship (Figure 6). The difference in MW (comparing PVA-A and PVA-C), created a minimal difference in MR T_2 relaxation times ≤ 5%. Comparing PVA-B and PVA-C showed that as the concentration was increased, the difference between the MR T_2 relaxation time increased with FTC.

Table 2: MR T_2 Relaxation times (mean ± SD) for PVA-A, B, and C, at concentrations of 10, 15, 17.5 and 20 % w/w.

%w/w	PVA-A		PVA-B		PVA-C		Increase in MW (A-C)	Increase in FTC (B-C)
	Mean (ms)	SD	Mean (ms)	SD	Mean (ms)	SD	% Mean difference	
10	117	0.8	119	5.2	123	3.6	5.1	3.4
15	90.2	1.1	86.0	2.6	90.3	1.0	0.1	5.0
17.5	82.8	0.4	70.0	1.5	82.2	1.3	-0.7	17.4
20	77.9	1.0	59.1	0.7	78.0	0.1	0.1	32.0

276

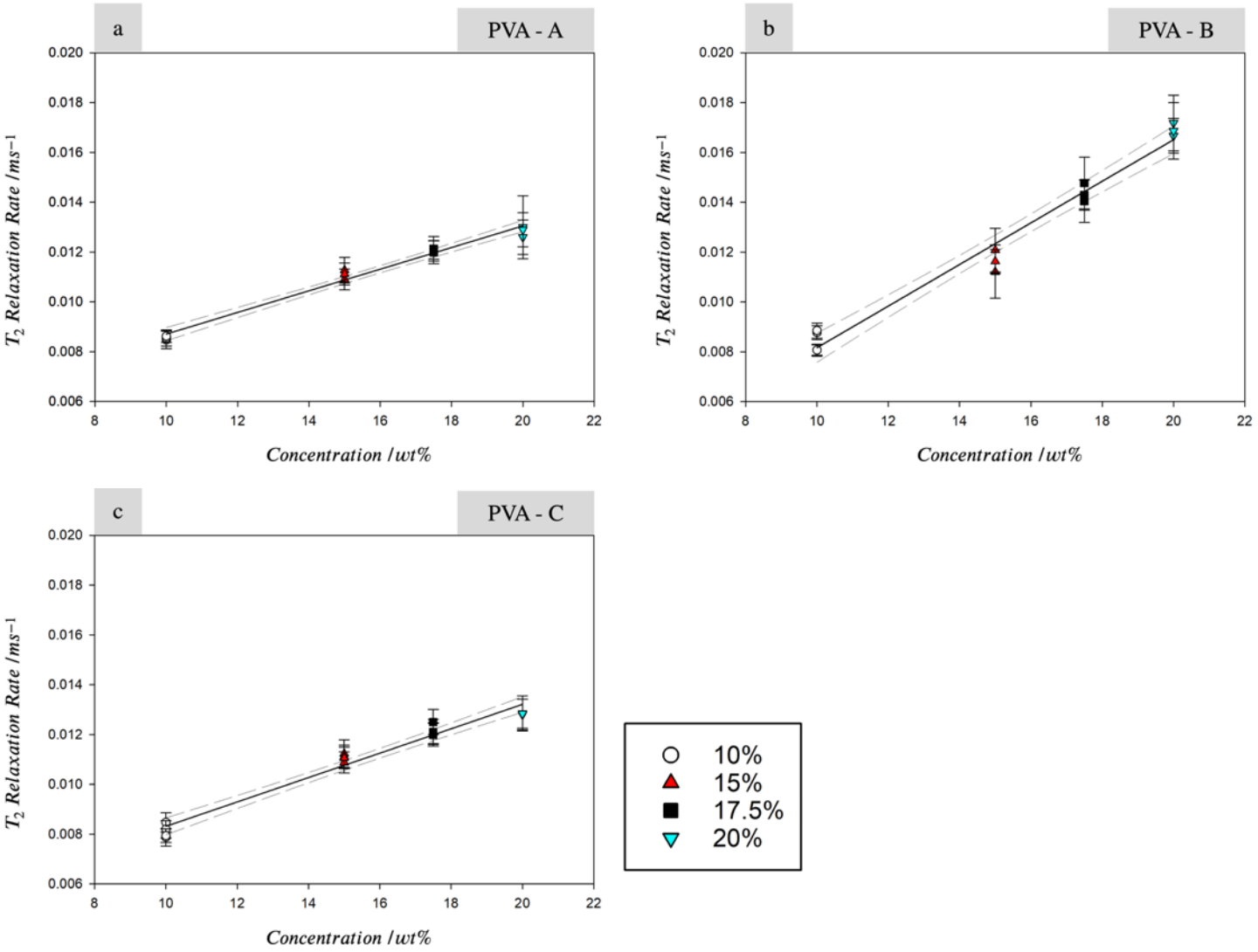

Figure 6: MR T_2 Relaxation Rate vs. concentration for PVA-A (a), PVA-B (b), and PVA-C (c). Points show average T_2 Relaxation Rate for each sample. Error bars show intra-sample standard deviation. Dashed lines show 95% confidence intervals for regression.

277

278 ***3.2.2 Freeze thaw cycles and MR T_2 relaxation time.***

279 An increase in the number of FTCs led to an increase in the mean MR T_2 relaxation time of a

280 sample, increasing from 101 ± 5.5 ms after one FTC, to 109 ± 8.6 ms after three FTCs (Table

281 3). A further increase to 122 ± 5.7 ms was seen after three days of equilibration in distilled

282 water. No clear trend can be see when analysing the change in inter-sample SD of the mean

283 with FTCs.

Figure 7 qualitatively demonstrates that the number of FTCs and further equilibrium altered the heterogeneity of samples. This observation is quantified by the increase in the mean intra sample standard deviation from 4.1% of the mean after 1 FTC, to 8.1% after 3 FTCs, and to 10.6% after equilibration (Table 3). This increase in the intra-sample variation can also be seen when analysing the distribution of MR T_2 relaxation times for all pixels within each relaxation map (Figure 8). The pixel distributions from three of the nine samples after 1 and 3 FTCs and after equilibration, are displayed, and a broader peak in MR T_2 distribution after 3 FTCs (Fig. 8b) can be observed, compared to the distribution after 1 FTC (Fig. 8a).

Table 3 shows the measurement of the sample cross-section from the MR T_2 relaxation map as an indicator of the change in sample shape after each step. This showed a decrease in area between 1 and 3 FTCs from 298 ± 6 mm^2 to 275 ± 4 mm^2, and a further decrease to 246 ± 4 mm^2 after three days of equilibration.

Table 3: MR T_2 Relaxation times for 10% w/w PVA at 1 and 3 freeze cycles, and after a further 3 days of equilibration. (n = 9 samples)

No. Freeze thaw cycles	Mean (ms)	Inter-sample SD of Means (ms)	Inter-sample SD of means (% of mean)	Mean of Intra-sample SDs (ms)	Mean Intra-sample SD (% of mean)	Mean Δ Cross-sectional area (mm^2)
1 (equivalent to PVA-B)	101	5.5	5.4	4.1	4.1	298 ± 6
3 (equivalent to PVA-C)	109	8.6	7.9	8.8	8.1	275 ± 4
3 + Equilibration	122	5.7	4.8	12.9	10.6	246 ± 4

300

301

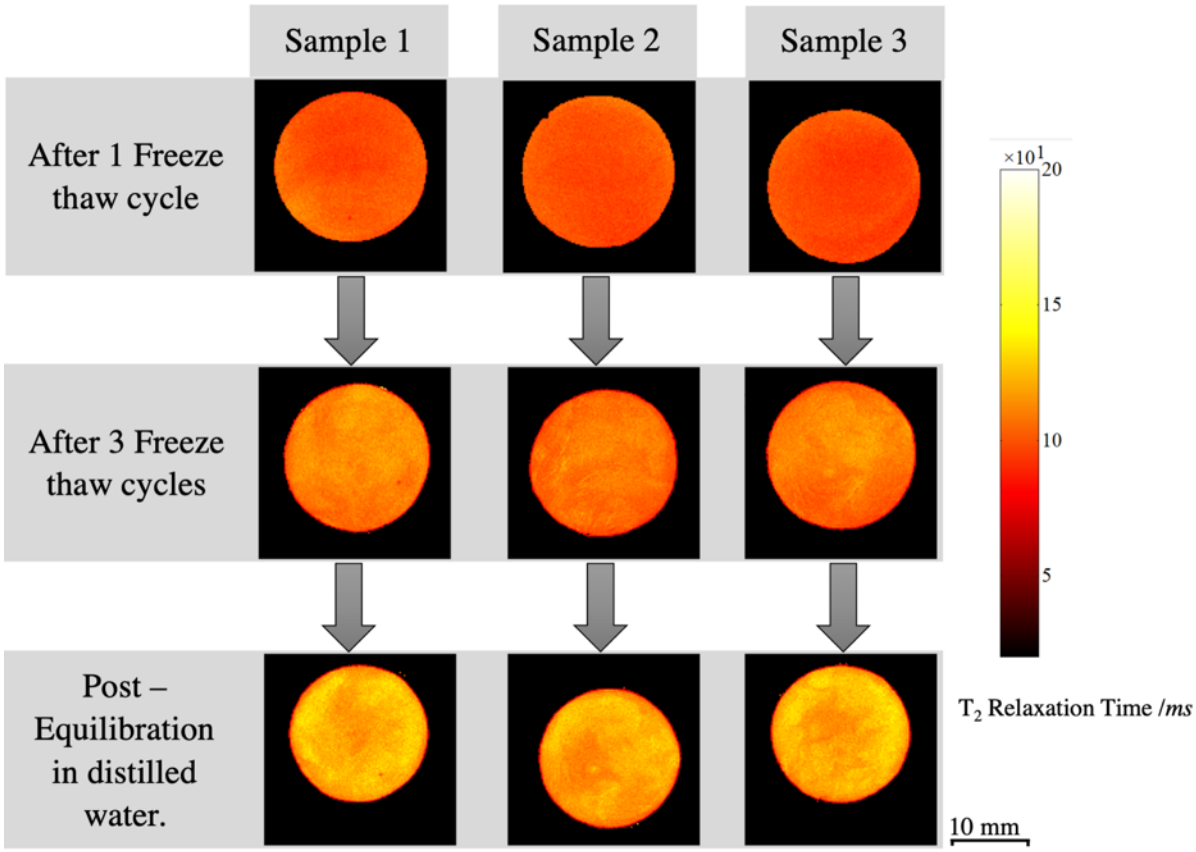

Figure 7: MR T_2 Relaxation maps of three samples of 146-186 kDa PVA with a concentration of 10% w/w, after 1 and 3 cycles, and after 3 days of storage in distilled water to allow for equilibration.

302

303

304

305

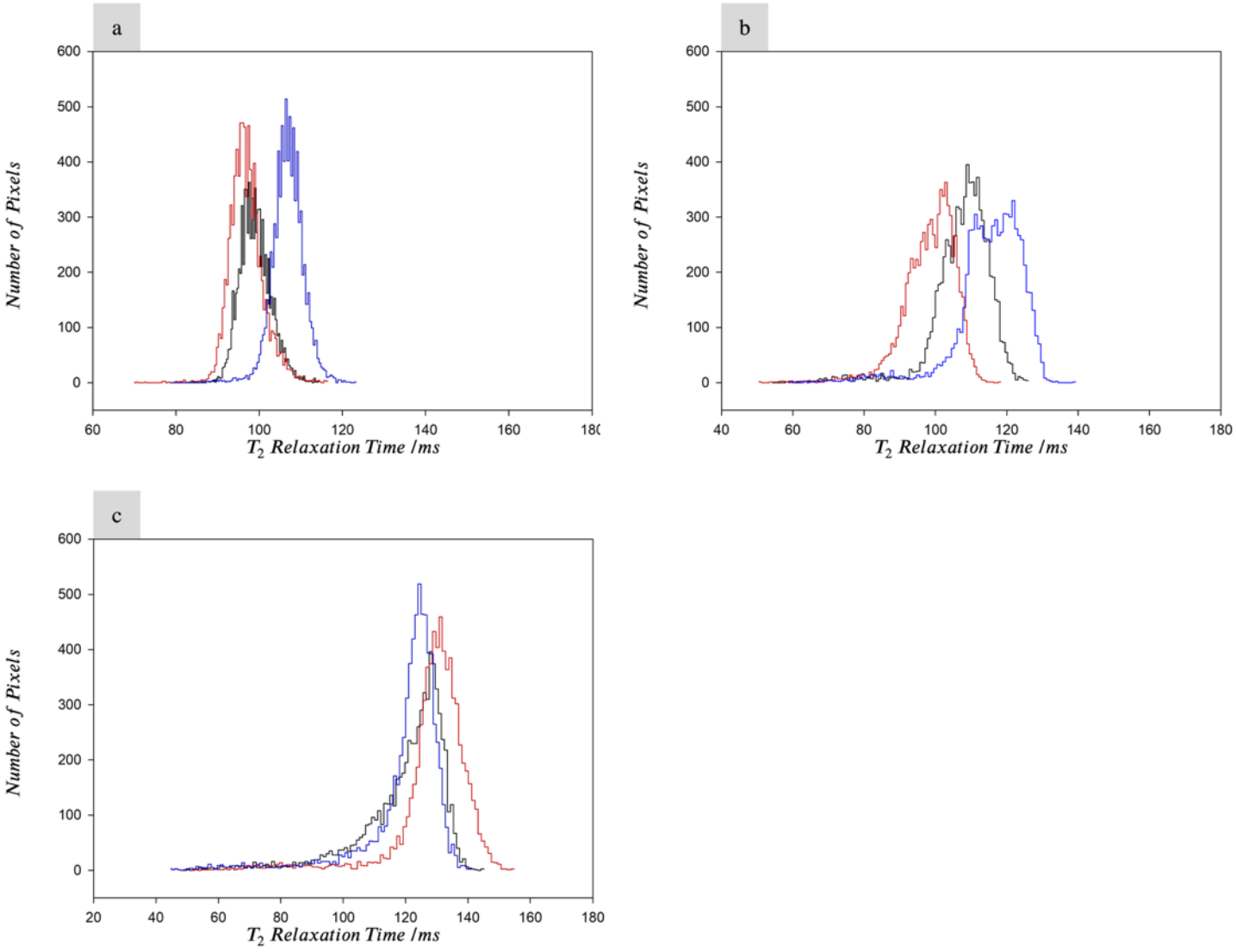

Figure 8: Histograms showing the distribution of MR T_2 relaxation time across all pixels for three samples after 1 (a) and 3 (b) freeze thaw cycle, and after a further 3 days of equilibration (c).

306

307

308 ***3.3 Viscoelastic properties and MR T_2 relaxation time.***

309 Based on the empirical evidence, the PVA-A data could be fitted to an exponential function

310 ($R^2 = 0.99$) between storage modulus and MR T_2 relaxation rate (Figure 9a). For PVA-B a

311 linear relationship ($R^2 = 0.95$) was empirically fitted (Figure 9b). For PVA-C it was not

312 possible to identify a correlation between storage modulus and MR T_2 relaxation rate;

313 therefore, no trend line has been fitted (Figure 9c). These trends (or lack of) were consistent

314 for all frequencies.

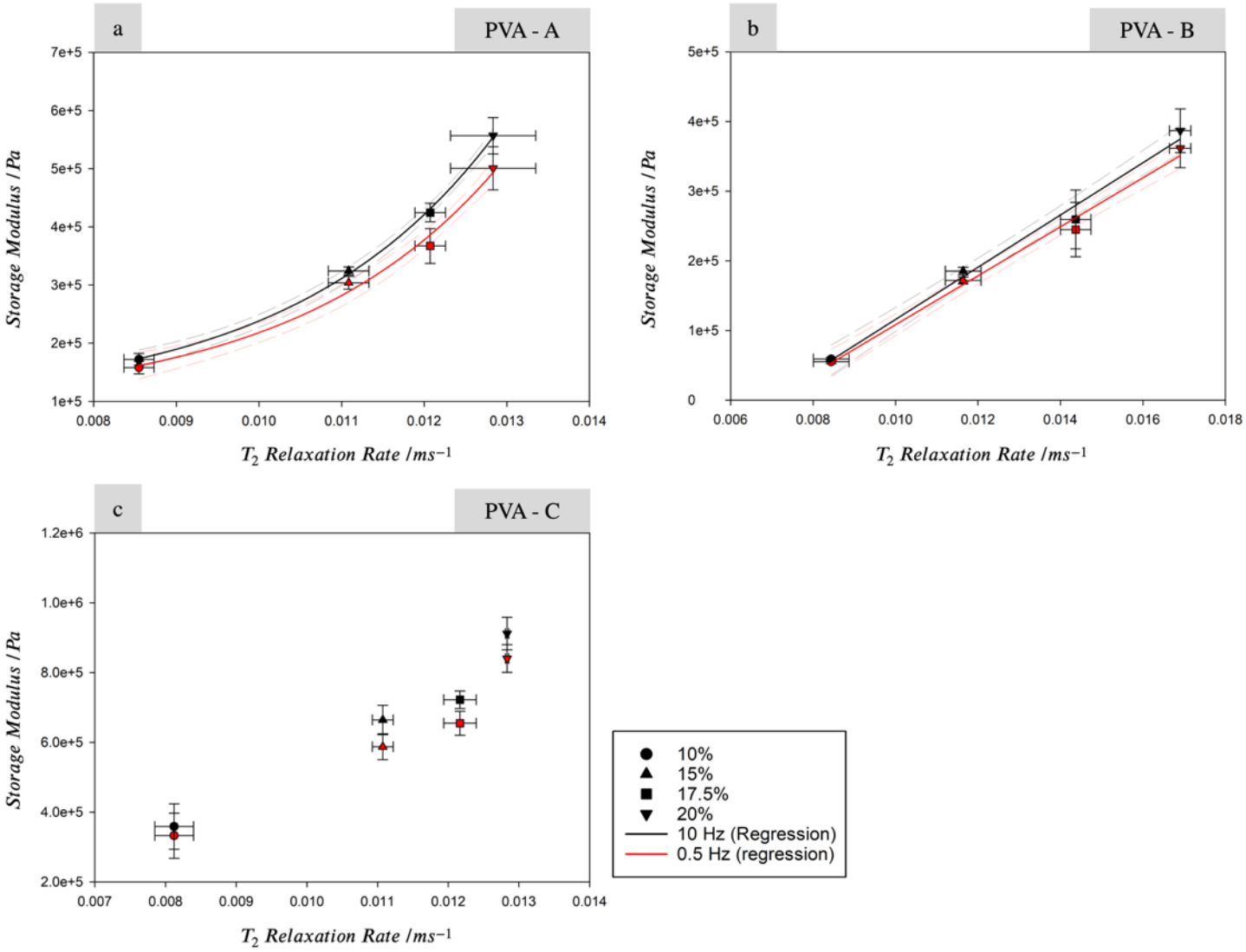

Figure 9: Storage Modulus plotted against MR T_2 Relaxation Rate for 0.5 Hz (red), and 10 Hz (black) for PVA-A (a), PVA-B (b), and PVA-C (c). Error bars show 95% confidence (n= 6). Regression lines for 0.5 Hz (red), and 10 Hz (black) are also given; dashed lines show 95% confidence intervals for regression.

315 For PVA-A, an exponential empirically-derived relationship was derived between loss

316 modulus and MR T_2 relaxation rate ($R^2 = 0.95$) (Figure 10a). It was also noted that the fit

317 appeared to improve as frequency decreased, with R^2 ranging from 0.98 at 0.5 Hz to 0.94 at

318 10 Hz. A linear relationship was observed between loss modulus and MR T_2 relaxation rate

319 for PVA-B ($R^2 = 0.88$) (Figure 10b). R^2 increased from 0.70 at 0.5 Hz to 0.94 at 10 Hz. As

320 with the comparison between storage modulus and MR T_2 relaxation rate for PVA-C, it was

not possible identify a correlation between loss modulus and MR T_2 Relaxation rate; therefore, no trendline has been presented (Figure 10c).

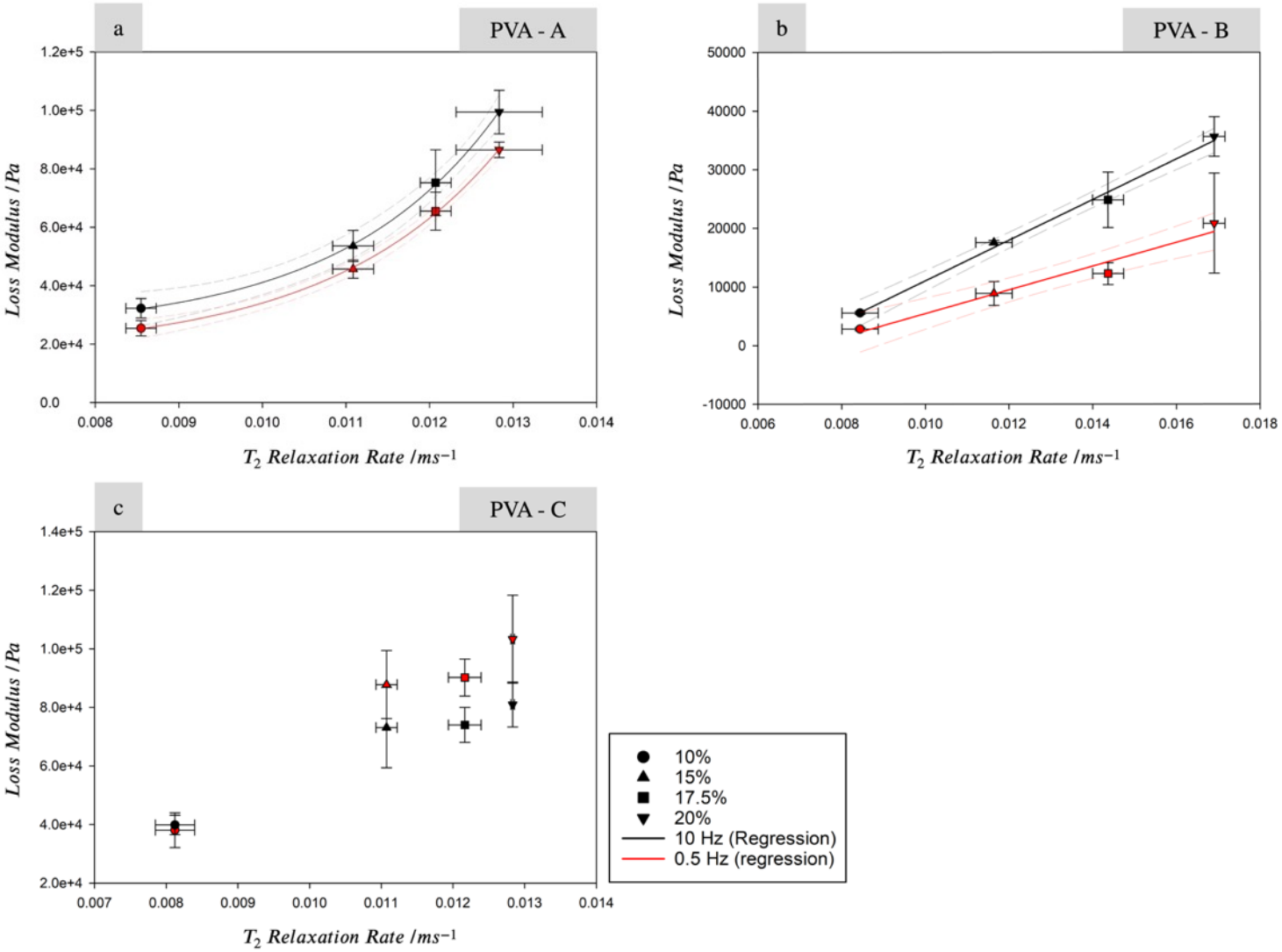

Figure 10: Loss Modulus plotted against MR T_2 Relaxation Rate for 0.5 Hz (red), and 10 Hz (black) for PVA-A (a), PVA-B (b), and PVA-C (c). Error bars show 95% confidence (n= 6). Regression lines for 0.5 Hz (red), and 10 Hz (black) are also given; dashed lines show 95% confidence intervals for regression.

4. Discussion

This study evaluated the effect of PVA concentration for two MWs, 1 and 3 FTCs on the dynamic viscoelastic properties, characterised using DMA, showing the potential to control the viscoelastic mechanical properties of PVA biomaterials by varying polymer composition and number of FTC. This study has also demonstrated the potential to link routine clinical

329 imaging to the material properties of PVA. For PVA-A and B, there was a statistically
330 significant correlation, between increasing concentration of the polymer and an increase in
331 the storage and loss moduli. The storage modulus was shown to increase with concentration
332 for PVA-C, however no statistically significant increase was seen in loss modulus between 15
333 and 20% ($p > 0.05$). Furthermore, the dynamic (complex) modulus increased with
334 concentration for all compositions. This increase in the parameters of viscoelasticity as
335 concentration is increased, is in agreement with previous literature, where a higher
336 concentration of PVA resulted in a higher Young's Modulus [34]. It was noted that for PVA-
337 C, that whilst a linear relationship was identified between complex modulus and
338 concentration, a non-linear relationship was identified between loss modulus and
339 concentration. As the concentration of PVA-C increases, the behaviour of the loss moduli
340 implies that the sample is storing a greater proportion of energy, to enable elastic recoil, and
341 therefore dissipating a lower proportion of energy. This behaviour is only occurring for PVA-
342 C samples, which are a higher MW composition, and have undergone 3 FTC.
343
344 Previous research, modelling the poro-viscoleastic properties of PVA, showed that it can be
345 described as a biphasic material [35]. However, in this study, the difference in viscoelastic
346 response with the proportion of water in the hydrogel, does not correlate with loss modulus
347 for all compositions i.e. PVA-C. Other studies have shown that as the concentration and MW
348 of PVA is increased, an increase in polymer cross-linking occurs during FTCs, resulting in a
349 denser polymer structure and a reduction in pore size [12], further resulting in an increase in
350 the mechanical stiffness of the hydrogel [34]. This hypothesis is further supported by the
351 behaviour of the viscoelastic properties presented in this study. An increase in crosslinking
352 present in PVA-C compared to PVA-B (due to an increase in FTCs) and PVA-A (due to
353 MW), increases the restriction on water movement in the samples due to an increase in in

polymerisation and decrease in pore size. It is hypothesised that this restriction on the water, reduces the hydrogel's ability to dissipate energy, as its freedom to flow out of the sample when a force is applied, will be reduced [36]. This theory is in agreement with several studies of the creep and stress relaxation properties of PVA; which have shown that as polymer concentration is increased, the response of creep and stress relaxation decreases [12, 35, 37]. This hypothesis would need to be tested on a wider range of MWs and FTCs, to confirm this theory. However, this study has shown that whilst compositional changes greatly affect the viscoelastic properties of PVA, the various parameters (for example concentration) do not affect different compositions in a consistent manner.

Miramini et al. [25] conducted a literature review to characterise the mechanical properties of connective tissue; this study yielded an elastic modulus (or equivalent) range of 0.09 – 10 MPa, 0.2 – 8 MPa and, 0.1 – 7 MPa for coronary, aortic, and femoral arteries respectively, and <1 – 170 MPa for articular cartilage. This range of values for connective tissue is extremely wide. Burton et al. [24] showed that the storage modulus of coronary arterial tissue is even higher (14.47 to 25.82 MPa). Yet, Holzapfel et al. [38] calculated the ultimate tensile stress of coronary arteries to be between 0.4 – 1.4 MPa. The values for the stiffest composition of PVA cryogel shown in this study, has a storage and loss moduli (0.8 MPa and 0.1 MPa respectively), which fall on the lower side of these reported literature values.

^{1}H MRI is able to map the distribution of hydrogen within a sample [39]. The lifetime of the MR signal, is dependent on two primary relaxation times, MR T_1 and MR T_2, which are sensitive to the chemical and physical environment of protons in a sample. In particular, both relaxation times are sensitive to molecular mobility and in the case of MR T_2 relaxation, the relaxation time decreases with decreasing mobility [39, 40]. Therefore, solids have typically

lower MR T_2 relaxation times compared to liquids. Additionally, MR T_2 relaxation time is also sensitive to chemical exchange and internal magnetic field gradients [41], in the presence of interfaces between materials of different magnetic susceptibilities, which is measured by MR T_2^* [39]. In the case of MRI, measured T_2 relaxation times can be sensitive to diffusion, to an extent dependent on the experimental imaging parameters. In this study, the imaging parameters were fixed throughout, and thus relative differences and trends can be identified.

This study evaluated the effect of PVA concentration for two MWs, 1 and 3 FTCs on MR T_2 relaxation time. It was found that MR T_2 relaxation time decreased as concentration was increased for PVA-A, B and C (Table 2). The reduction in MR T_2 relaxation time, and thus signal, correlates with the reduction in the %wt. of water in the samples. This result is in agreement with Orr et al. [30]. The additional parameters assessed in this study, identified further trends. There was an increase in MR T_2 relaxation time with FTC, which contradicts the trend reported by Chu and Rutt [29]. Table 2 also identifies that the difference in MR T_2 relaxation time, between 1 and 3 FTCs, increases with the concentration (previously unreported). Table 3 shows that there was a reduction in cross-sectional area with the FTCs and subsequent equilibrium process, which further aligns with results from [29], and is attributed to water being expelled by crystallite growth. The robustness of the observations between FTCs and MR T_2 relaxation time are inherently limited due to two discrete data points. Whilst it potentially identifies two novel trends, these require further investigation to establish correlation and statistical significant. Nevertheless, some observations can be made about research methodology, and hypotheses can be drawn based on scientific insight.

MRI was able to qualitatively and quantitatively assess the change in sample heterogeneity with manufacturing protocol, showing that an increase in FTCs results in an increased pixel

distribution of MR T_2 relaxation time throughout a sample (Table 3, Figure 7 and 8). Figure 8 also shows a deviation from normal distribution after equilibration, with a skew to lower values of MR T_2 relaxation times. In part, this can be attributed to the 'halo' of lower signal intensity around the edge of the samples (Figure 7), which further agrees with the expulsion of water described by Chu et al. [29], occurring at the boundary of the sample. The literature reports that increasing the number of FTCs during manufacture, results in compositional heterogeneity within the hydrogel [42]. This is due to the formation of ice crystals during the freezing process, resulting in an increase in the concentration of the polymer solution in surrounding regions and promoting more interactions between the polymer chains, and between the polymer and ice crystals [43]. Thawing of the ice crystals, results in pockets of water, which can lead to a microporous structure throughout the hydrogel. Subsequent FTCs reinforce this process, which results in the formation of polymer rich and polymer poor regions [42, 44].

The generation of water pockets, and increased mobility of the water molecules, in the microstructure of the material is hypothesised to cause the increase in MR T_2 relaxation time with FTC. It is important to emphasise, that the increase in MR T_2 relaxation time with FTC, is attributed to an increase in water mobility, as opposed to water concentration, which through the cross-sectional area results in Table 3 and [29] was assumed to reduce. This observation is further strengthened by Table 2, which shows (by comparing PVA-B and PVA-C) that by reducing %wt. water concentration, has less impact than the increase in water mobility from additional FTCs. To confirm the microstructural changes of the PVA with FTC requires further investigation. The phase heterogeneity of PVA has been previously measured using different experimental methods, including X-ray diffraction [45], small angle neutron scattering [46, 47], and confocal laser scanning microscopy [48]. MRI is not able to resolve

429 the microscopic pore structure of PVA however, this study has demonstrated that the
430 formation of polymer-rich and polymer-poor regions can be indirectly measured through the
431 resulting variation in polymer and water content of these regions and thus the signal. It is
432 unlikely that this microscopic variation in composition has an impact on the viscoelastic
433 properties of the hydrogels, as these are bulk measurements.
434
435 Comparing Tables 2 and 3, the mean MR T_2 relaxation time for 10% PVA-C in Table 2
436 (123ms) is equivalent to 10% PVA-C after 3 days of equilibrating in water in Table 3
437 (122ms). Reflecting on the difference in methodology between these experiments, the
438 difference in MR T_2 relaxation time pre and post equilibration (~10%), demonstrates the
439 critical importance of the storage conditions of PVA cryogels. This parameter was not
440 reported in [29], and was approximately 4 weeks in [30]. Chu and Rutt [29] also described
441 different manufacturing and imaging protocol, most notably, they state long echo times,
442 which would increase susceptibility to internal magnetic field gradients. To robustly
443 determine the source of the opposing trends between MR T_2 relaxation time and FTC reported
444 in [29] and this study an increased and more detailed assessment of manufacturing
445 parameters, under matched imaging parameters, would be required.
446
447 Finally and importantly, this paper has demonstrated, for the first time, a correlation between
448 viscoelastic mechanical properties and the MR T_2 relaxation time for a defined composition.
449 Note that “correlation does not imply causation”, and in this case both the viscoelastic and
450 MRI properties of PVA are dependent on the hydrogel’s water content. The mechanical
451 properties and MR T_2 relaxation time of PVA are correlated because both are affected by
452 changes in PVA composition. This unique result is exciting because it suggests the possibility
453 of MRI based quantification of the composition-dependent mechanical properties of PVA.

Such a development would have huge ramifications in the development and application of tissue scaffolds, implants and phantoms. Future development and validation could allow in-situ and non-invasive imaging of the mechanical function of PVA cryogels, with the wider principles outlined in this paper also applicable to other biocompatible hydrogels [49]. Magnetic resonance elastography (MRE) is currently the most researched method used to measure mechanical properties *in vivo*, with PVA being a commonly used phantoms material to develop MRE [50]. The techniques presented here could be used to enhance and validate such developments by using *in vivo* imaging to validate mechanical properties and monitor changes in homogeneity in a sample or implant.

The advent of more advanced manufacturing techniques for hydrogels, such as additive manufacture, leads to the ability to create more complex geometries, [18] and multi-material models [51, 52]. The findings from this study have the potential to aid such developments by demonstrating how to alter, and control, the mechanical properties of PVA by varying the composition of the polymer and the parameters of additive manufacturing [53]. These advances imply the potential for considerably more accurate material models for soft connective tissues, allowing for changing mechanical properties throughout an implant or phantom [54]. More specifically, this study demonstrates the feasibility of optimising the viscoelastic material properties of PVA based on this hydrogel's composition. Therefore, allowing the results shown in this study to be used in tandem with more complex manufacturing methods, to further tune the mechanical behaviour of PVA. This information will also allow researchers to be more informed when selecting materials, such as for medical devices or imaging phantoms, and has applications to further improve the accuracy of material models of PVA. For example, the frequency domain data presented in this study is

478 available for the analysis of stress of medical devices which use PVA [9, 55, 56] under
479 dynamic loading conditions which mimic physiological loading [57].
480
481 This study has successfully shown the impact of the compositional and manufacturing
482 parameters of PVA cryogel on its viscoelastic properties and MR T_2 relaxation time. Future
483 research will require an increased number of parameters to explore the impact on the loss
484 modulus and MR T_2 relaxation time. Further to this, an increased number of FTCs would be
485 required to increase the dynamic moduli of the cryogel to the equivalent range for some
486 arterial tissue reported in the literature.
487
488 ***Conclusion***
489 This study has explored the effect of MW, concentration and the manufacturing protocol of
490 PVA cryogel on its viscoelastic mechanical properties and the MR T_2 Relaxation time. It was
491 shown that:
492 - An increase in concentration results in an increase in storage and loss moduli.
493 - The trend between concentration and viscoelastic moduli is dependent on the MW and
494 the manufacturing protocol.
495 - A linear relationship exists between MR T_2 relaxation rate and concentration,
496 inclusive of both MWs and variations in manufacturing protocol.
497 - MRI can qualitatively and quantitatively identify sample heterogeneity, which was
498 shown to increase with number of FTCs and further equilibrating in water.

499 Further to these results, this research demonstrated a causal relationship between the MR T_2
500 relaxation rate and viscoelastic properties of PVA. Excitingly, this demonstrates the potential
501 to image the composition-dependent viscoelastic properties of PVA remotely. Such an attribute

could enable future in-situ and non-invasive identification of the mechanical properties of implants, tissue scaffolds and phantoms.

6. Acknowledgements

JC is currently funded by an Engineering and Physical Sciences Research Council scholarship (EP/N509590/1). The materials and testing equipment used in this study was funded by an Arthritis Research UK grant (H0671; now part of Versus Arthritis).

7. Conflict of Interest

The authors declare that there is no conflict of interest.

8. References

1. Muppalaneni, S. and H. Omidian, *Polyvinyl Alcohol in Medicine and Pharmacy: A Perspective*. Journal of Developing Drugs, 2013. ***02***(03): p. 1-5. DOI: 10.4172/2329-6631.1000112

2. Alves, M.H., et al., *Poly(vinyl alcohol) physical hydrogels: new vista on a long serving biomaterial*. Macromol Biosci, 2011. ***11***(10): p. 1293-313. DOI: 10.1002/mabi.201100145

3. Luengo-Fernandez, R., et al., *Cost of cardiovascular diseases in the United Kingdom*. Heart, 2006. ***92***(10): p. 1384-9. DOI: 10.1136/hrt.2005.072173

4. *Cardiovascular Disease: A costly burden for America*. 2017: American Heart Association.URL: https://www.heart.org/-/media/files/get-involved/advocacy/burden-report-technical-report.pdf?la=en - *Date accessed*: June 2021.

5. *British Heart Foundation Statistics Factsheet - UK*. 2021 (March): British Heart Foundation.URL: https://www.bhf.org.uk/what-we-do/our-research/heart-statistics - *Date accessed*: June 2021.

6. Singh, J.A., et al., *Rates of Total Joint Replacement in the United States: Future Projections to 2020-2040 Using the National Inpatient Sample*. J Rheumatol, 2019. ***46***(9): p. 1134-1140. DOI: 10.3899/jrheum.170990

7. Cournane, S., et al., *Assessment of the accuracy of an ultrasound elastography liver scanning system using a PVA-cryogel phantom with optimal acoustic and mechanical properties*. Phys Med Biol, 2010. ***55***(19): p. 5965-83. DOI: 10.1088/0031-9155/55/19/022

8. Chatelin, S., et al., *Anisotropic polyvinyl alcohol hydrogel phantom for shear wave elastography in fibrous biological soft tissue: a multimodality characterization*. Phys Med Biol, 2014. ***59***(22): p. 6923-40. DOI: 10.1088/0031-9155/59/22/6923

9. Jiang, H., et al., *Design and manufacture of a polyvinyl alcohol (PVA) cryogel tri-leaflet heart valve prosthesis*. Med Eng Phys, 2004. ***26***(4): p. 269-77. DOI: 10.1016/j.medengphy.2003.10.007

10. Wan, W.K., et al., *Optimizing the tensile properties of polyvinyl alcohol hydrogel for the construction of a bioprosthetic heart valve stent*. J Biomed Mater Res, 2002. ***63***(6): p. 854-61. DOI: 10.1002/jbm.10333

11. Millon, L.E., C.J. Oates, and W. Wan, *Compression properties of polyvinyl alcohol--bacterial cellulose nanocomposite*. J Biomed Mater Res B Appl Biomater, 2009. ***90***(2): p. 922-9. DOI: 10.1002/jbm.b.31364

12. Wong, E.Y.L. and D.W. Wan, *Poly (vinyl alcohol) nanocomposite hydrogels for intervertebral disc prostheses*. Electronic Thesis and Dissertation Repository, 2012. ***731***. DOI: https://ir.lib.uwo.ca/etd/731

13. Oka, M., et al., *Development of artificial articular cartilage*. Proc Inst Mech Eng H, 2000. ***214***(1): p. 59-68. DOI: 10.1243/0954411001535246

14. Oka, M., et al., *Synthetic osteochondral replacement of the femoral articular surface*. J Bone Joint Surg Br, 1997. ***79***(6): p. 1003-7. DOI: 10.1302/0301-620x.79b6.7606

15. Noguchi, T., et al., *Poly(vinyl alcohol) hydrogel as an artificial articular cartilage: evaluation of biocompatibility*. J Appl Biomater, 1991. ***2***(2): p. 101-7. DOI: 10.1002/jab.770020205

16. Pan, Y.-S., D.-S. Xiong, and R.-Y. Ma, *A study on the friction properties of poly(vinyl alcohol) hydrogel as articular cartilage against titanium alloy*. Wear, 2007. ***262***(7-8): p. 1021-1025. DOI: 10.1016/j.wear.2006.10.005

17. Baker, M.I., et al., *A review of polyvinyl alcohol and its uses in cartilage and orthopedic applications*. J Biomed Mater Res B Appl Biomater, 2012. ***100***(5): p. 1451-7. DOI: 10.1002/jbm.b.32694

18. Tan, Z., et al., *Cryogenic 3D Printing of Super Soft Hydrogels*. Sci Rep, 2017. ***7***(1): p. 16293. DOI: 10.1038/s41598-017-16668-9

19. Malone, A.J., et al., *Polyvinyl alcohol cryogel based vessel mimicking material for modelling the progression of atherosclerosis*. Phys Med, 2020. ***69***(December 2019): p. 1-8. DOI: 10.1016/j.ejmp.2019.11.012

20. Fromageau, J., et al., *Characterization of PVA cryogel for intravascular ultrasound elasticity imaging*. IEEE Trans Ultrason Ferroelectr Freq Control, 2003. ***50***(10): p. 1318-24. DOI: 10.1109/tuffc.2003.1244748

21. Seale Lej, T., K. P, and H. L, *Magnetic Resonance Elastography through Atherosclerosis: A Feasibility Study*. Journal of Clinical & Experimental Cardiology, 2016. ***7***(12). DOI: 10.4172/2155-9880.1000481

22. Lawless, B.M., et al., *Viscoelastic properties of a spinal posterior dynamic stabilisation device*. J Mech Behav Biomed Mater, 2016. ***59***: p. 519-526. DOI: 10.1016/j.jmbbm.2016.03.011

23. Lawless, B.M., et al., *Viscoelasticity of articular cartilage: Analysing the effect of induced stress and the restraint of bone in a dynamic environment*. J Mech Behav Biomed Mater, 2017. ***75***(May): p. 293-301. DOI: 10.1016/j.jmbbm.2017.07.040

24. Burton, H.E., J.M. Freij, and D.M. Espino, *Dynamic Viscoelasticity and Surface Properties of Porcine Left Anterior Descending Coronary Arteries*. Cardiovasc Eng Technol, 2017. ***8***(1): p. 41-56. DOI: 10.1007/s13239-016-0288-4

25. Miramini, S., et al., *The status and challenges of replicating the mechanical properties of connective tissues using additive manufacturing*. J Mech Behav Biomed Mater, 2020. ***103***: p. 103544. DOI: 10.1016/j.jmbbm.2019.103544

26. Kosukegawa, H., et al., *Measurements of Dynamic Viscoelasticity of Poly (vinyl alcohol) Hydrogel for the Development of Blood Vessel Biomodeling*. Journal of Fluid Science and Technology, 2008. ***3***(4): p. 533-543. DOI: 10.1299/jfst.3.533

27. Park, J.-S., J.-W. Park, and E. Ruckenstein, *On the viscoelastic properties of poly(vinyl alcohol) and chemically crosslinked poly(vinyl alcohol)*. Journal of Applied Polymer Science, 2001. ***82***(7): p. 1816-1823. DOI: 10.1002/app.2023

28. Hadj Henni, A., et al., *Hyper-frequency viscoelastic spectroscopy of biomaterials*. J Mech Behav Biomed Mater, 2011. ***4***(7): p. 1115-22. DOI: 10.1016/j.jmbbm.2011.03.020

29. Chu, K.C. and B.K. Rutt, *Polyvinyl Alcohol Cryogel An Ideal Phantom Material for MR Studies of Arterial Flow and Elasticity*. Magn Reson Med, 1997. ***37***(2): p. 314-9. DOI: 10.1002/mrm.1910370230

30. Orr, T.N., et al. *A Phantom Material for Mri of the Neonatal Brain*. in *CMBES Proceedings*. 2007. URL: https://proceedings.cmbes.ca/index.php/proceedings/article/view/178

31. Baxter, J., K.G. Buchan, and D.M. Espino, *Viscoelastic properties of mitral valve leaflets: An analysis of regional variation and frequency-dependency*. Proc Inst Mech Eng H, 2017. ***231***(10): p. 938-944. DOI: 10.1177/0954411917719741

32. Constable, M., et al., *Effect of glutaraldehyde based cross-linking on the viscoelasticity of mitral valve basal chordae tendineae,*. Biomed Eng Online, 2018. ***17***(1): p. 93. DOI: 10.1186/s12938-018-0524-2

33. Sadeghi, H., D.E.T. Shepherd, and D.M. Espino, *Effect of the variation of loading frequency on surface failure of bovine articular cartilage*. Osteoarthritis Cartilage, 2015. ***23***(12): p. 2252-2258. DOI: 10.1016/j.joca.2015.06.002

34. Gupta, S., S. Goswami, and A. Sinha, *A combined effect of freeze--thaw cycles and polymer concentration on the structure and mechanical properties of transparent PVA gels*. Biomed Mater, 2012. ***7***(1): p. 015006. DOI: 10.1088/1748-6041/7/1/015006

35. Liu, K. and T.C. Ovaert, *Poro-viscoelastic constitutive modeling of unconfined creep of hydrogels using finite element analysis with integrated optimization method*. J Mech Behav Biomed Mater, 2011. ***4***(3): p. 440-50. DOI: 10.1016/j.jmbbm.2010.12.005

36. Wan, W., et al., *Poly(Vinyl Alcohol) Cryogels for Biomedical Applications*. Advances in Polymer Science, 2014. DOI: 10.1007/978-3-319-05846-7_8

37. Stammen, J.A., et al., *Mechanical properties of a novel PVA hydrogel in shear and unconfined compression*. Biomaterials, 2001. ***22***(8): p. 799-806. DOI: 10.1016/s0142-9612(00)00242-8

38. Holzapfel, G.A., et al., *Determination of layer-specific mechanical properties of human coronary arteries with nonatherosclerotic intimal thickening and related constitutive modeling*. Am J Physiol Heart Circ Physiol, 2005. ***289***(5): p. H2048-58. DOI: 10.1152/ajpheart.00934.2004

39. Britton, M.M., *MRI of chemical reactions and processes*. Prog Nucl Magn Reson Spectrosc, 2017. ***101***: p. 51-70. DOI: 10.1016/j.pnmrs.2017.03.001

40. Britton, M.M., *Magnetic resonance imaging of chemistry*. Chem Soc Rev, 2010. ***39***(11): p. 4036-43. DOI: 10.1039/b908397a

41. Cimmarusti, G.M., et al., *Characterization of Open-Cell Sponges via Magnetic Resonance and X-ray Tomography*. Materials (Basel), 2021. ***14***(9): p. 2187. DOI: 10.3390/ma14092187

42. Hassan, C.M. and N.A. Peppas, *Structure and applications of poly(vinyl alcohol) hydrogels produced by conventional crosslinking or by freezing/thawing methods*. Advances in Polymer Science, 2000. ***153***: p. 37-65. DOI: 10.1007/3-540-46414-x_2

43. Yokoyama, F., et al., *Morphology and structure of highly elastic poly(vinyl alcohol) hydrogel prepared by repeated freezing-and-melting*. Colloid & Polymer Science, 1986. ***264***(7): p. 595-601. DOI: 10.1007/bf01412597

44. Hassan, C.M. and N.A. Peppas, *Structure and Morphology of Freeze/Thawed PVA Hydrogels*. Macromolecules, 2000. ***33***(7): p. 2472-2479. DOI: 10.1021/ma9907587

45. Ricciardi, R., et al., *X-ray Diffraction Analysis of Poly(vinyl alcohol) Hydrogels, Obtained by Freezing and Thawing Techniques*. Macromolecules, 2004. ***37***(5): p. 1921-1927. DOI: 10.1021/ma035663q

46. Kanaya, T., et al., *Structure of Poly(vinyl alcohol) Gels Studied by Wide- and Small-Angle Neutron Scattering*. Macromolecules, 2002. ***27***(20): p. 5609-5615. DOI: 10.1021/ma00098a014

47. Millon, L.E., et al., *SANS Characterization of an Anisotropic Poly(vinyl alcohol) Hydrogel with Vascular Applications*. Macromolecules, 2007. ***40***(10): p. 3655-3662. DOI: 10.1021/ma062781f

48. Fergg, F., F.J. Keil, and H. Quader, *Investigations of the microscopic structure of poly(vinyl alcohol) hydrogels by confocal laser scanning microscopy*. Colloid and Polymer Science, 2001. ***279***(1): p. 61-67. DOI: 10.1007/s003960000398

49. Meakin, J.R., et al., *Thermal analysis of poly(2-hydroxyethyl methacrylate) (pHEMA) hydrogels*. Journal of Materials Science: Materials in Medicine, 2003. ***14***(1): p. 9-15. DOI: 10.1023/A:1021589017753

50. Thomas-Seale, L.E., et al., *A simulation of the magnetic resonance elastography steady state wave response through idealised atherosclerotic plaques*. IAENG International Journal of Computer Science, 2011. ***38***(4): p. 394-400.

51. Kolesky, D.B., et al., *3D Bioprinting of Vascularized, Heterogeneous Cell-Laden Tissue Constructs*. Advanced Materials, 2014. ***26***(19): p. 3124-3130. DOI: https://doi.org/10.1002/adma.201305506

52. Khalil, S., J. Nam, and W. Sun, *Multi-nozzle deposition for construction of 3D biopolymer tissue scaffolds*. Rapid Prototyping Journal, 2005.

53. Crolla, J.P., et al., *The orthotropic viscoelastic characterisation of sub-zero 3D-printed poly(vinyl alcohol) cryogel*. MRS Advances, 2021. DOI: 10.1557/s43580-021-00086-1

54. Leijten, J., et al., *Spatially and temporally controlled hydrogels for tissue engineering*. Materials Science and Engineering: R: Reports, 2017. ***119***: p. 1-35.

55. Simsek, G.M., et al., *PVA/gelatin-based hydrogel coating of nickel-titanium alloy for improved tissue-implant interface*. Applied Physics A, 2021. ***127***(5): p. 387. DOI: 10.1007/s00339-021-04542-5

56. Na, H., et al., *Fabrication of PVDF/PVA microtubules by coaxial electrospinning*. Polymer, 2012. ***53***(13): p. 2736-2743. DOI: https://doi.org/10.1016/j.polymer.2012.04.021

57. Li, W., D.E. Shepherd, and D.M. Espino, *Dynamic mechanical characterization and viscoelastic modeling of bovine brain tissue*. Journal of the Mechanical Behavior of Biomedical Materials, 2021. ***114***: p. 104204.

Supplementary data:

Table S1: Storage Modulus (Mean ± SD) for all PVA-A samples tested at frequencies between 0.5-10 Hz.

Freq. (Hz)	Storage Modulus (Pa)							
	10% W/W		15% W/W		17.5% W/W		20% W/W	
	Mean	SD	Mean	SD	Mean	SD	Mean	SD
0.5	158000	9500	298000	5500	362000	16000	484000	24000
1	159000	8400	301000	3900	373000	15000	501000	22000
2	163000	8500	308000	4700	388000	14000	518000	24000
3	165000	8600	312000	5200	397000	13000	529000	25000
4	167000	8600	315000	5400	404000	13000	535000	26000
6	169000	8700	319000	5800	414000	13000	546000	26000
8	171000	8800	323000	5900	421000	14000	552000	27000
10	172000	8800	324000	5900	425000	14000	557000	27000

Table S2: Storage Modulus (Mean ± SD) for all PVA-B samples tested at frequencies between 0.5-10 Hz.

Freq. (Hz)	Storage Modulus (Pa)							
	10% W/W		15% W/W		17.5% W/W		20% W/W	
	Mean	SD	Mean	SD	Mean	SD	Mean	SD
0.5	55000	2400	172000	4400	245000	36000	361000	25000
1	55700	2200	175000	4800	247000	36000	367000	27000
2	56600	2200	177000	4900	251000	37000	373000	27000
3	57100	2200	179000	5000	253000	37000	376000	28000
4	57500	2300	180000	5000	254000	37000	378000	28000
6	58100	2300	183000	5100	256000	38000	382000	28000
8	58500	2300	184000	5200	258000	38000	385000	28000
10	58900	2300	185000	5200	259000	39000	387000	29000

Table S3: Storage Modulus (Mean ± SD) for all PVA-C samples tested at frequencies between 0.5-10 Hz.

Freq. (Hz)	Storage Modulus (Pa)							
	10% W/W		15% W/W		17.5% W/W		20% W/W	
	Mean	SD	Mean	SD	Mean	SD	Mean	SD
0.5	333000	59000	588000	34000	655000	31000	840000	36000
1	336000	59000	605000	35000	674000	30000	862000	39000
2	343000	60000	627000	37000	692000	28000	883000	40000
3	348000	60000	639000	37000	702000	27000	892000	41000
4	350000	60000	646000	38000	708000	26000	898000	41000
6	355000	60000	656000	38000	715000	25000	906000	42000
8	357000	60000	661000	38000	720000	24000	909000	42000
10	359000	59000	664000	38000	722000	23000	912000	43000

Table S4: Loss Modulus (Mean ± SD) for all PVA-A samples tested at frequencies between 0.5-10 Hz.

Freq. (Hz)	Loss Modulus (Pa)			
	10% W/W	15% W/W	17.5% W/W	20% W/W

	Mean	SD	Mean	SD	Mean	SD	Mean	SD
0.5	25400	2300	45700	2700	65500	5700	86500	2300
1	26400	2100	46600	2700	67600	6400	88200	3800
2	27200	2400	47400	2900	69200	7900	89300	5100
3	28000	2400	47900	3400	70300	8900	90200	5500
4	28700	2400	48700	3800	70800	9400	91200	5600
6	29900	2700	50100	4200	71800	9800	93500	5900
8	31200	2800	51800	4600	72900	9800	96200	6200
10	32300	2900	53600	4600	75300	9800	99400	6500

Table S5: Loss Modulus (Mean ± SD) for all PVA-B samples tested at frequencies between 0.5-10 Hz.

Freq. (Hz)	Loss Modulus (Pa)							
	10% W/W		15% W/W		17.5% W/W		20% W/W	
	Mean	SD	Mean	SD	Mean	SD	Mean	SD
0.5	2820	240	8890	1800	12300	1700	20900	7800
1	2980	200	8920	890	12800	1900	19700	5100
2	3260	160	9670	550	13800	2200	20400	3500
3	3550	150	10700	420	15200	2500	22100	2900
4	3820	150	11700	370	16600	2800	24000	2800
6	4410	170	13700	300	19400	3300	27900	2700
8	4990	180	15600	310	22200	3900	31700	2900
10	5550	210	17600	340	24800	4300	35700	3100

Table S6: Loss Modulus (Mean ± SD) for all PVA-C samples tested at frequencies between 0.5-10 Hz.

Freq. (Hz)	Loss Modulus (Pa)							
	10% W/W		15% W/W		17.5% W/W		20% W/W	
	Mean	SD	Mean	SD	Mean	SD	Mean	SD
0.5	38100	5400	87800	11000	90200	5800	103000	14000
1	38700	4900	87100	13000	85300	6000	95000	10000
2	37900	3900	81900	15000	78400	7000	84700	10000
3	37400	3400	77800	15000	74800	7100	79700	9500
4	37300	3100	75000	15000	72600	7000	77200	9000
6	37700	2700	72300	14000	71300	6500	76100	8000
8	38600	2800	71900	13000	72000	5900	77800	7400
10	39900	3000	73100	13000	74000	5500	81000	7000

Table S7: Storage and Loss constants with respect to concentration of PVA-A and PVA-B for frequencies between 0.5 and 10 Hz. (Equations 7 & 8)

	Freq. (Hz)	Storage Modulus (Pa)				Loss Modulus (Pa)			
		a_s	b_s	d_s	R^2	a_l	b_l	d_l	R^2
PVA-A	0.5	-86400	108000	0.083	0.98	-1640	8080	0.12	0.97
	1	-70600	94800	0.09	0.98	-2170	8690	0.117	0.97
	2	-75700	97400	0.09	0.98	-2780	9390	0.115	0.95
	3	-76400	98000	0.091	0.99	-1630	9140	0.116	0.94
	4	-86700	104000	0.089	0.99	157	8550	0.119	0.94
	6	-99200	113000	0.087	0.99	3480	7460	0.125	0.93
	8	-108000	118000	0.086	0.99	6680	6470	0.132	0.93
	10	-103000	115000	0.087	0.99	7360	6510	0.133	0.94
PVA-B	0.5	-92000	48700	0.114	0.96	-339	536	0.183	0.94
	1	-89000	46800	0.114	0.96	-2320	1330	0.14	0.83
	2	-88700	46800	0.114	0.96	-4360	2390	0.117	0.9
	3	-91600	48000	0.114	0.96	-5950	3260	0.107	0.92
	4	-91600	48000	0.114	0.96	-7560	4160	0.101	0.93
	6	-90700	47900	0.114	0.96	-9720	5360	0.0973	0.94
	8	-91600	48500	0.114	0.96	-12000	6640	0.0941	0.94
	10	-90300	47600	0.112	0.96	-13600	7500	0.0939	0.93

Table S8: Storage constants with respect to concentration of PVA-C for frequencies between 0.5 and 10 Hz. (Equation 9)

	Freq. (Hz)	f	g	R^2
PVA-C	0.5	-167000	53200	0.93
	1	-171000	50600	0.94
	2	-174000	51900	0.94
	3	-174000	52400	0.94
	4	-173000	52700	0.94
	6	-170000	53000	0.94
	8	-168000	53100	0.94
	10	-158000	48700	0.93

Table S9: Mean MR T_2 relaxation rate constants for PVA-A. B. and C. (Equation 10)

	x	y	R^2
PVA-A	0.0040	0.00043	0.99
PVA-B	-0.00020	0.00080	0.99
PVA-C	0.0034	0.00050	0.97

Table S10: Multiplication factors comparing variation of viscoelastic properties when MW is increased from 89-98 kDa to 146-186 kDa (10-20% PVA-A and C) between frequencies of 0.5 and 10 Hz.

Freq. (Hz)	Storage Modulus (Pa)				Loss Modulus (Pa)			
	10% W/W	15% W/W	17.5% W/W	20% W/W	10% W/W	15% W/W	17.5% W/W	20% W/W
0.5	2.1 ×	2.0 ×	1.8 ×	1.7 ×	1.5 ×	2.0 ×	1.4 ×	1.2 ×
1	2.1 ×	2.0 ×	1.8 ×	1.7 ×	1.5 ×	1.9 ×	1.3 ×	1.1 ×
2	2.1 ×	2.0 ×	1.8 ×	1.7 ×	1.4 ×	1.7 ×	1.1 ×	0.93 ×
3	2.1 ×	2.1 ×	1.8 ×	1.7 ×	1.3 ×	1.6 ×	1.1 ×	0.87 ×
4	2.1 ×	2.1 ×	1.7 ×	1.7 ×	1.3 ×	1.5 ×	1.0 ×	0.83 ×
6	2.1 ×	2.1 ×	1.7 ×	1.7 ×	1.3 ×	1.4 ×	1.0 ×	0.80 ×
8	2.1 ×	2.1 ×	1.7 ×	1.7 ×	1.2 ×	1.4 ×	1.0 ×	0.80 ×
10	2.1 ×	2.1 ×	1.7 ×	1.6 ×	1.2 ×	1.4 ×	1.0 ×	0.80 ×
Average	***2.1 ×***	***2.0 ×***	***1.8 ×***	***1.7 ×***	***1.2 ×***	***1.6 ×***	***1.1 ×***	***0.91 ×***
SD	***0.0083***	***0.027***	***0.039***	***0.033***	***0.094***	***0.21***	***0.14***	***0.14***

Table S11: Multiplication factors comparing variation of viscoelastic properties when the number of freeze thaw cycles is increased from 1 to 3 (10-20% PVA-B and C) between frequencies of 0.5 and 10 Hz.

Freq. (Hz)	Storage Modulus (Pa)				Loss Modulus (Pa)			
	10% W/W	15% W/W	17.5% W/W	20% W/W	10% W/W	15% W/W	17.5% W/W	20% W/W
0.5	6.1 ×	3.4 ×	2.7 ×	2.3 ×	14 ×	9.9 ×	7.3 ×	4.9 ×
1	6.0 ×	3.5 ×	2.7 ×	2.3 ×	13 ×	9.8 ×	6.7 ×	4.8 ×
2	6.1 ×	3.5 ×	2.8 ×	2.4 ×	12 ×	8.5 ×	5.7 ×	4.2 ×
3	6.1 ×	3.6 ×	2.8 ×	2.4 ×	11 ×	7.3 ×	4.9 ×	3.6 ×
4	6.1 ×	3.6 ×	2.8 ×	2.4 ×	9.8 ×	6.4 ×	4.4 ×	3.2 ×
6	6.1 ×	3.6 ×	2.8 ×	2.4 ×	8.5 ×	5.3 ×	3.7 ×	2.7 ×
8	6.1 ×	3.6 ×	2.8 ×	2.4 ×	7.7 ×	4.6 ×	3.2 ×	2.5 ×
10	6.1 ×	3.6 ×	2.8 ×	2.4 ×	7.2 ×	4.2 ×	3.0 ×	2.3 ×
Average	***6.1 ×***	***3.5 ×***	***2.8 ×***	***2.4 ×***	***10 ×***	***7.0 ×***	***4.9 ×***	***3.5 ×***
SD	***0.026***	***0.063***	***0.039***	***0.015***	***2.2***	***2.1***	***1.5***	***0.97***

Table S12: Storage and loss constants with respect to MR T_2 relaxation rate of PVA-A for frequencies between 0.5 and 10 Hz. (Equations 11 & 13)

Freq. (Hz)	Storage Modulus (Pa)				Loss Modulus (Pa)			
	a_s	b_s	d_s	R^2	a_l	b_l	d_l	R^2
0.5	86800	2680	388	0.98	17000	119	496	0.98
1	91100	2200	406	0.98	17500	130	491	0.97
2	91900	2210	409	0.98	17900	143	485	0.95
3	93400	2180	412	0.98	18800	137	488	0.94
4	91900	2340	408	0.99	19800	124	496	0.94
6	90600	2530	404	0.99	21600	102	511	0.93
8	89600	2670	401	0.99	23400	83.2	528	0.93
10	92000	2560	405	0.99	24400	82.8	531	0.94

Table S13: Storage and loss constants with respect to MR T_2 relaxation rate of PVA-B for frequencies between 0.5 and 10 Hz. (Equations 12 and 14)

Freq. (Hz)	Storage Modulus (Pa)			Loss Modulus (Pa)		
	a_s	b_s	R^2	a_l	b_l	R^2
0.5	-243000	35200000	0.95	-14900	2030000	0.70
1	-247000	35700000	0.95	-13500	1910000	0.82
2	-250000	36200000	0.95	-13500	1970000	0.89
3	-252000	36500000	0.95	-14500	2130000	0.92
4	-254000	36700000	0.95	-15700	2320000	0.92
6	-256000	37000000	0.95	-18400	2700000	0.93
8	-257000	37300000	0.95	-20900	3080000	0.94
10	-259000	37500000	0.95	-23500	3460000	0.94